

MODELING THE EFFECTS OF DUST ON GALACTIC SPECTRAL ENERGY DISTRIBUTIONS FROM THE ULTRAVIOLET TO THE MILLIMETER BAND

LAURA SILVA

International School for Advanced Studies, SISSA, Trieste, Italy

GIAN LUIGI GRANATO AND ALESSANDRO BRESSAN

Osservatorio Astronomico di Padova, Padova, Italy

AND

LUIGI DANESE

International School for Advanced Studies, SISSA, Trieste, Italy

Received 1998 March 16; accepted 1998 July 16

ABSTRACT

We present models of photometric evolution of galaxies in which the effects of a dusty interstellar medium have been included with particular care. A chemical evolution code follows the star formation rate, the gas fraction, and the metallicity, basic ingredients for the stellar population synthesis. The latter is performed with a grid of integrated spectra of simple stellar populations (SSP) of different ages and metallicities, in which the effects of dusty envelopes around asymptotic giant branch (AGB) stars are included. The residual fraction of gas in the galaxy is divided into two phases: the star-forming molecular clouds and the diffuse medium. The relative amount is a model parameter. The molecular gas is subdivided into clouds of given mass and radius: it is supposed that each SSP is born within the cloud and progressively escapes it. The emitted spectrum of the star-forming molecular clouds is computed with a radiative transfer code. The diffuse dust emission (cirrus) is derived by describing the galaxy as an axially symmetric system, in which the local dust emissivity is consistently calculated as a function of the local field intensity due to the stellar component. Effects of very small grains, subject to temperature fluctuations, as well as polycyclic aromatic hydrocarbons (PAHs) are included. The model is compared and calibrated with available data of normal and starburst galaxies in the local universe, in particular new broadband and spectroscopic *Infrared Space Observatory* (ISO) observations. It will be a powerful tool to investigate the star formation, the initial mass function (IMF), supernova rate (SNR) in nearby starbursts and normal galaxies, as well as to predict the evolution of luminosity functions of different types of galaxies at wavelengths covering four decades.

Subject headings: dust, extinction — galaxies: ISM — galaxies: spiral — galaxies: starburst — infrared: galaxies — radiative transfer

1. INTRODUCTION

Observations performed in the last decade or so, particularly in the IR regime, have clearly demonstrated that dust, which contains a large fraction of heavy elements ejected from stars, is one of the most important components of the interstellar medium (ISM). This paper is mainly concerned with the influence of dust grains on the transfer of radiation emitted by stellar systems. Basically dust absorbs and scatters photons, mostly at wavelengths $\lesssim 1 \mu\text{m}$, and returns to the radiation field the subtracted energy in the form of IR photons. The resulting spectral energy distribution (SED) is often substantially changed and in many relevant cases radically modified.

Not surprisingly, dust reprocessing of the optical-UV photons emitted by stars into the infrared regime turns out to be particularly severe in galaxies undergoing massive episodes of star formation, which preferentially occur within dense molecular clouds. Indeed dust could affect galaxy evolution because it modifies the physical and chemical conditions of the ISM. In particular star formation is at least favored by the presence of dust, which shields dense clouds from stellar UV radiation and keeps them to temperatures low enough to allow the onset of gravitational instability.

The SED of normal star-forming disklike galaxies is also affected by dust, mainly associated with the diffuse ISM and

with the envelopes of evolved asymptotic giant branch (AGB) stars. As for early-type systems, it has been suggested often that the first episode of massive star formation could be essentially hidden to optical searches owing to dust reprocessing, since the ISM of these systems might have been metal enriched on a very short timescale, the lifetime of the first generation of massive stars (Franceschini et al. 1994, and references therein; Cimatti et al. 1997). Even local quiescent elliptical galaxies exhibit infrared emission (e.g., Jura 1986; Bally & Thronson 1989; Knapp et al. 1989; Roberts et al. 1991) and visual dust obscuration (e.g., Veron-Cetty & Veron 1988; Kim 1989; Goudfrooij et al. 1994), which arises in part from dust grains continuously formed in dusty outflows from AGB stars (Tsai & Mathews 1996; Bressan, Granato, & Silva 1998), as well as molecular line emission (e.g., Gordon 1990; Roberts et al. 1991; Lees et al. 1991). Overall, a direct comparison of the luminosity functions of galaxies in the optical and in the far-IR shows that, locally, about 30% of starlight is dust reprocessed.

At least three different dusty environments must be taken into account in order to properly understand the UV to submillimeter properties of galaxies: (1) dust in interstellar H I clouds heated by the general interstellar radiation field (ISRF) of the galaxy (the “cirrus” component), (2) dust associated with star-forming molecular clouds and H II regions, and (3) circumstellar dust shells produced by the

windy final stages of stellar evolution. These environments have different importance in different galactic systems at various evolutionary stages.

Despite this, in many papers dealing with the spectrophotometric evolution of galaxies the radiative processes occurring in a dusty interstellar medium were originally neglected (e.g., Bruzual & Charlot 1993 and Leitherer & Heckman 1995, the former the most adopted one to interpret data on different galaxy types, the latter appositely built for starburst galaxies). Indeed their codes are nowadays commonly used together with some prescription to approximate the effects of the ISM. In other cases (e.g., Guiderdoni & Rocca-Volmerange 1987; Mazzei, De Zotti, & Xu 1994; Lançon & Rocca-Volmerange 1996; Fioc & Rocca-Volmerange 1997), the effects of dust are included only partially and/or with substantial simplifications. For instance often extinction is considered but thermal reradiation is not, or scattering is neglected, or not all the relevant dusty environments are considered, or optically thin emission is assumed, or an unrealistic geometry is adopted. Those works facing a complete computation of the radiative transfer through a dusty medium do not include it in the more general framework of galaxy evolution but are instead interested either in the interpretation of single objects (e.g., Krügel & Siebenmorgen 1994) or in understanding the effects of dust geometry on the extinction of the emerging spectrum (e.g., Bruzual, Magris, & Calvet 1988; Witt, Thronson, & Capuano 1992; Cimatti et al. 1997; Wise & Silva 1996; Bianchi, Ferrara, & Giovanardi 1996; Gordon, Calzetti, & Witt 1997).

The inclusion of dust effects into spectrophotometric codes leads to many difficulties. Although the integrated photometric properties of a hypothetical dust-free galaxy are geometry independent, dust introduces a strong dependence on the distribution of both stars and ISM. Moreover the optical properties of dust grains and their dependence on environmental conditions have not yet been fully explored and understood. The ensuing uncertainty may only be parametrized to some extent. The effects of scattering, absorption, and emission of grains, which may not be in radiative equilibrium with the radiation field, complicate the solution of the integrodifferential transfer equation in a complex geometry.

Nonetheless a more realistic and complete computation of the spectrophotometric galaxy models including dust is required, since neglecting the complexity of the dust effects can lead to erroneous estimates of many interesting quantities such as the star formation rate (SFR). Also, the estimate of the age of a galaxy through the fit of its broadband SED is hampered by the degeneracy between the colors of an old galaxy and those of an extinguished young galaxy (e.g., Cimatti et al. 1997), further complicating the well-known age-metallicity degeneracy.

We have therefore developed chemospectrophotometric self-consistent galactic models including dust. Three different dusty environments are considered: envelopes of AGB stars, molecular star-forming clouds, and diffuse ISM; the dust model is comprehensive of normal big grains, small thermally fluctuating grains, and polycyclic aromatic hydrocarbon (PAH) molecules; for each grain family, the appropriate computation of absorption and reemission is performed. The models are suited to simulate galaxies of any Hubble type in different evolutionary stages, since we include the possibility of different geometrical distributions

both for stars and gas. The complete radiative transfer equation is numerically solved whenever necessary.

The many parameters and uncertainties introduced by the presence of dust can be constrained only by means of the multiband approach pursued in this paper, where the spectrophotometric properties of galaxies are consistently reproduced from the UV to the submillimeter, i.e., taking into account extinction at short wavelengths and the consequent thermal emission in the IR regime. The combination of observations from *HST*, Keck, *Infrared Space Observatory (ISO)*, and ground-based optical, IR, and submillimeter telescopes already provided several objects at significant redshift with spectral information on this large λ range. Their number will increase after the completion of *ISO* surveys and will burst when *SIRTF*, *FIRST*, *Planck Surveyor*, and *NGST* operate.

In this paper we present the model and we use it to study local galaxies. In a forthcoming paper we will use it to study the cosmic evolution of different types of galaxies.

2. MODEL DESCRIPTION

We divide the problem of estimating the SED of a galaxy at age t_G , including dust effects, in two steps: (1) the history of the star formation rate $\Psi(t)$, of the initial mass function (IMF), of the metallicity $Z(t)$, and of the residual gas fraction $g(t)$ is determined and then (2) the integrated SED of the galaxy is predicted taking into account all the stars and the gas present at t_G . When the effects of dust are neglected, step (2) simply involves a sum of all the spectra of stars. In our case we have instead to introduce a specific geometry for gas and stars and then to compute the radiative transfer of the radiation emitted by the stars and the dust.

The purpose of the present work is mainly to develop a general procedure for step (2). Step (1) includes a number of possible choices that can be easily interfaced to our code in order to describe the evolution of the SED.

2.1. Chemical Evolution

The chemical evolution is a preliminary process in our code. We summarize here the main aspects of the code, which basically follows the guidelines given by Tantaló et al. (1996).

The code describes one-zone open models including the infall of primordial gas [$\dot{M}(t) \propto \exp(-t/t_{\text{inf}})$], in order to simulate the collapse phase of galaxy formation and, when required by the astrophysical situation under study, galactic winds.

The adopted SFR is a Schmidt-type law, i.e., proportional to some power (between 1 and 2) of the available gas mass: $\Psi(t) = v M_g(t)^k$. For starburst galaxies we add to the general smooth SFR one or more bursts of star formation. As for the IMF we used the usual Salpeter law: $\Phi(M) \propto M^{-x}$, with $x = 2.35$. The upper limit of the mass range is fixed to $100 M_\odot$.

This kind of chemical evolution model has been successfully tested against nearby spheroidal galaxies and also well reproduces the properties of different types of galaxies with appropriate choices of the parameters (e.g., a quiet spiral-type evolution is well mimicked with a low value of v and/or a long infall timescale, see Matteucci 1996 for a thorough review).

2.2. Synthesis of Starlight Spectrum (Including Dusty Envelopes of AGB Stars)

The library of isochrones for the simple stellar populations (SSP), the building blocks of galaxy models, is based on the Padua stellar models (Bertelli et al. 1994) with a major difference, which consists in the computation of the effects of dusty envelopes around AGB stars. The SSPs span a wide range in age, from 1 Myr to 20 Gyr, and in metallicity, $Z = 0.004, 0.008, 0.02, 0.05, 0.1$, to realistically reproduce the mix of age and composition of the stellar content of galaxies. The inclusion of a wide range of metallicity is imposed by the aim of comparing model estimates to the excellent data available even for young high-redshift galaxies.

The spectral synthesis technique for the starlight alone consists in summing up the spectra of each stellar generation provided by the SSP of the appropriate age and metallicity weighted by the SFR at time of the star's birth (e.g., Bressan, Chiosi, & Fagotto 1994).

Effects of dust in the envelopes of evolved stars are usually neglected in the synthesis of a composite population. This is not justified for intermediate age population clusters, whose brightest tracers are AGB stars, and/or in a wide-wavelength synthesis approach. To overcome this limitation, we computed new isochrones and SSPs in which, along the AGB, a suitable dusty envelope is assumed to surround the star. For this envelope the radiative transfer is solved by means of the code described by Granato & Danese (1994). The envelope parameters, in particular its optical thickness, which is straightforwardly linked to the mass-loss rate and to the expansion velocity, are derived as a function of basic stellar parameters (mass, luminosity, radius, and metallicity) combining hydrodynamic model results and empirical relations. A detailed description of the adopted procedure can be found in Bressan et al. (1998).

2.3. Geometry

As already pointed out, the dust effects on SEDs depend on the relative distribution of stars and dust. The assumed geometry is sketched in Figure 1. The galaxy is approximated as a system having azimuthal symmetry, as well as planar symmetry with respect to the equatorial plane. We

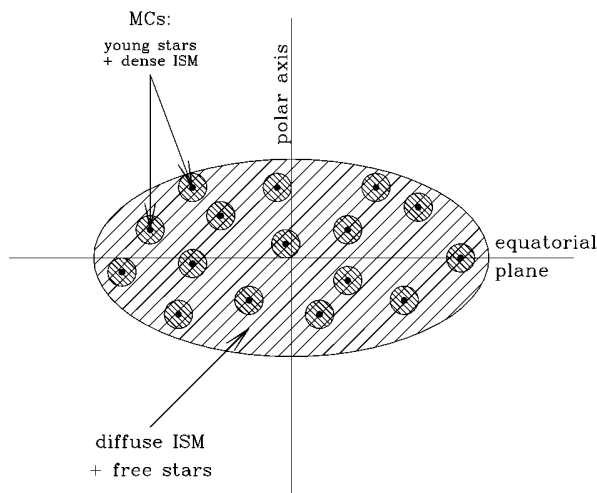


FIG. 1.—Scheme of the components included in our model computations and their adopted geometry.

take into account three components: (1) star-forming molecular clouds complexes, hereafter MCs, comprising dusty gas in a dense phase, H II regions and very young stars embedded in it (young stellar objects [YSOs]); (2) stars already escaped from these dense clouds (henceforth *free stars*); (3) diffuse gas (cirrus).

We work in spherical coordinates (r, θ, ϕ) . The densities of the three components ρ_{mc} , ρ_* , and ρ_c , respectively, depend on r and θ through analytical laws. In the following, unless otherwise explicitly stated, ρ_{mc} and ρ_* have identical spatial dependence. In order to describe disklike galaxies, we use a double exponential of the distance from the polar axis $R = r \sin \theta$ and from the equatorial plane $z = r \cos \theta$:

$$\rho = \rho_0 \exp(-R/R_d) \exp(-|z|/z_d). \quad (1)$$

In the code the scale lengths R_d and z_d can be independently set for the three components, but in the models presented in this paper (§ 3) we simply adopt identical values for them. In other words we use two adjustable parameters when describing disklike galaxies: $R_d^* = R_d^{mc} = R_d^c$ and $z_d^* = z_d^{mc} = z_d^c$. Observations within our Galaxy suggest $z_d^* \sim 0.35$ kpc. As a reference the e -folding scale length is related to the absolute magnitude by

$$\log_{10}(R_d/\text{kpc}) \sim -0.2M_B - 3.45 \quad (2)$$

(Im et al. 1995).

In the case of spheroidal systems we adopt for both stars and dust spherical symmetric distributions with King profile:

$$\rho = \rho_0 [1 + (r/r_c)^2]^{-\gamma}, \quad (3)$$

extended up to the tidal radius r_t . This truncation radius is required in King models since $M(r)$, the mass contained within r , diverges as $r \rightarrow \infty$. Our results are not very sensitive to its precise choice; thus, we simply adopted the standard value $\log(r_t/r_c) = 2.2$. As for the stellar component we simply set $\gamma = 3/2$. It has been suggested that the core radius r_c correlates with the luminosity (Binggeli, Sandage, & Tarenghi 1984):

$$\log_{10}\left(\frac{r_c}{\text{kpc}}\right) \sim \begin{cases} -0.3(M_B + 22.45) & \text{if } M_B \leq -20, \\ -0.1(M_B + 27.34) & \text{if } M_B > -20. \end{cases} \quad (4)$$

The distribution of dust in spheroidal systems is poorly known, but it has been suggested that $\rho_{\text{dust}} \propto \rho_{\text{stars}}^n$ with $n \simeq \frac{1}{2} - \frac{1}{3}$ (Froehlich 1982; Witt et al. 1992; Wise & Silva 1996), i.e., $\gamma \simeq 0.5 - 0.75$. In other words the dust distribution seems to be less concentrated than that of stars. In particular an additional cool component located in the outer parts has been invoked to explain *IRAS* observations (Tsai & Mathews 1996).

The volume emissivity ($\text{ergs cm}^{-3} \text{ s}^{-1} \text{ sr}^{-1} \text{ \AA}^{-1}$) of the galaxy at each point is the sum of three terms arising respectively from the three components listed above:

$$j_\lambda = j_\lambda^{mc} + j_\lambda^* + j_\lambda^c. \quad (5)$$

In the following sections we will describe how these quantities, as well as the specific flux measured by an external observer, are computed. A preliminary step is to define the optical properties of dust.

2.4. The Dust Model

Once the geometrical arrangement is specified, the effects

of dust on radiative transfer depend on physical and chemical properties of grains, which affect the way they absorb and emit photons. It is expected and observationally well established that these properties are functions of the particular environment in which grains happen to live. Several populations may be distinguished (see Dorschner & Henning 1995 for a review): (1) stellar outflow dust (further subdivided into the two chemical subgroups of carbon-rich and oxygen-rich dust), (2) dust in the diffuse ISM, (3) dust in molecular clouds and dust around YSOs. As for stellar outflow dust, we refer to the treatment of Bressan et al. (1998) mentioned above. Here we discuss our choices for the other two dusty components of the model galaxy.

Although many efforts have been devoted to derive a so-called *standard* model for dust in the diffuse ISM, its precise composition remains controversial. Significant clues can be derived from observations. The prominent features observed in its spectrum at 9.7 and 18 μm indicate the presence of silicate grains. Conversely, the origin of the 2175 \AA feature is somewhat debated, although graphite still stands as the most attractive solution (see Mathis 1990). The emission bands in the 3–13 μm region indicate the presence of PAHs (Puget, Léger, & Boulanger 1985), which together with small thermally fluctuating grains contribute also to produce the warm mid-IR cirrus emission. Therefore we included these components in our diffuse dust model. We adopted the same mixture even for MCs, for which the information is scanty, only decreasing the fraction of PAH molecules (see below).

The optical properties of silicate and graphite grains have been computed by Laor & Draine (1993) for spherical shapes using Mie theory, the Rayleigh-Gans approximation, and geometric optics. In particular we used the cross sections of graphite and silicate grains computed by B. T. Draine for 81 grain sizes from 0.001 to 10 μm in logarithmic steps $\delta \log a = 0.05$.¹

In order to get the overall radiative properties of the dust mixture, the abundance and the size distribution of grains must be specified. We started from the distribution proposed by Draine & Lee (1984, hereafter DL), which is tuned on the optical-UV extinction law of the galactic diffuse ISM. On the other hand, DL pointed out that their model displays significant discrepancies with extinction data above 2 μm and that these discrepancies are not surprising, since observations at longer wavelength tend to sample lines of sight through denser clouds, where grain population may differ from that present in more diffuse regions.

A more severe limitation of DL model is that the mid-IR (MIR) cirrus emission at wavelengths $\lambda \leq 60 \mu\text{m}$ is not reproduced (Fig. 3) because grains are always large enough to maintain a low temperature thermal equilibrium in the general ISRF. This emission requires reprocessing of the field by particles, very small grains, and/or PAH molecules, reaching temperatures higher than those attained with equilibrium heating (e.g., Puget et al. 1985; Draine & Anderson 1985; Dwek et al. 1997). This requirement can be matched by decreasing the lower limit of the graphite grain distribution. Since these grains must be more numerous than the simple extrapolation of the DL power law, a break to a steeper power law is introduced below a_b . These adjustments to the DL model enhance the MIR cirrus emission but tend to degrade the agreement with the observed extinc-

tion law in the optical-UV region. However, a reasonable compromise can be found. For graphite grains we adopted the following size distribution:

$$\frac{dn_i}{da} = \begin{cases} A_i n_H a^{\beta_1} & \text{if } a_b < a < a_{\max}, \\ A_i n_H a_b^{\beta_1 - \beta_2} a^{\beta_2} & \text{if } a_{\min} < a < a_b, \end{cases} \quad (6)$$

with $a_{\min} = 8 \text{\AA}$, $a_{\max} = 0.25 \mu\text{m}$, $a_b = 50 \text{\AA}$, $\beta_1 = -3.5$, $\beta_2 = -4.0$, and $A_g = 10^{-25.22} \text{ cm}^{2.5} \text{ H}^{-1}$. As for silicate grains, we maintained the same size distribution as DL. As a result, 282 atoms per million H (ppM) of C are locked in dust grains.

In the code the size distributions has been discretized in 20 logarithmic bins following the prescriptions given by Draine & Malhotra (1993). Once the bathing radiation field is specified, the emissivity of grains with radius $a > 100 \text{\AA}$ is computed assuming that they achieve thermal equilibrium, so that all grains of a given composition and radius emit as graybodies at a single temperature. Below this limit a temperature distribution for each size bin and composition is computed following Guhathakurta & Draine (1989), and then the emissivity is obtained by integrating over this distribution.

To model the observed IR emission occurring in bands at 3.3, 6.2, 7.7, 8.6, and 11.3 μm we include also a population of planar PAHs. The optical-UV absorption cross section σ_{PAH} is reported in Figure 2. This has been obtained by averaging the cross sections of six different PAH mixtures measured by Léger et al. (1989b) above 1200 \AA , and smoothly joining the resulting mean curve to the coronene cross section below this limit. The same cross section is used to take into account the effects of PAH on the extinction curve, assuming a vanishing albedo (Fig. 3). Désert, Boulanger, & Puget (1990) have proposed an analytical description of σ_{PAH} derived from the observed interstellar extinction curve in the 1200–3300 \AA range, under the assumption that these particles dominate its extreme UV (EUV) rise. On the other hand the EUV rise can be ascribed

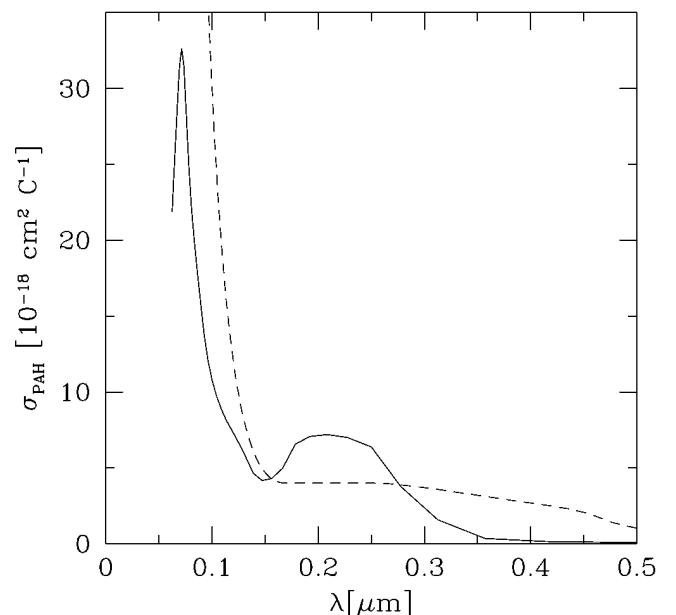


FIG. 2.—Solid line: Cross section of PAH per carbon atom, derived from laboratory measurements taken from Léger et al. (1989b). Dashed line: The analytical law assumed by Désert et al. (1990) for molecule with $N_C = 50$ C atoms (N_C controls the cutoff above 0.3 μm).

¹ Made available via anonymous ftp at astro.princeton.edu.

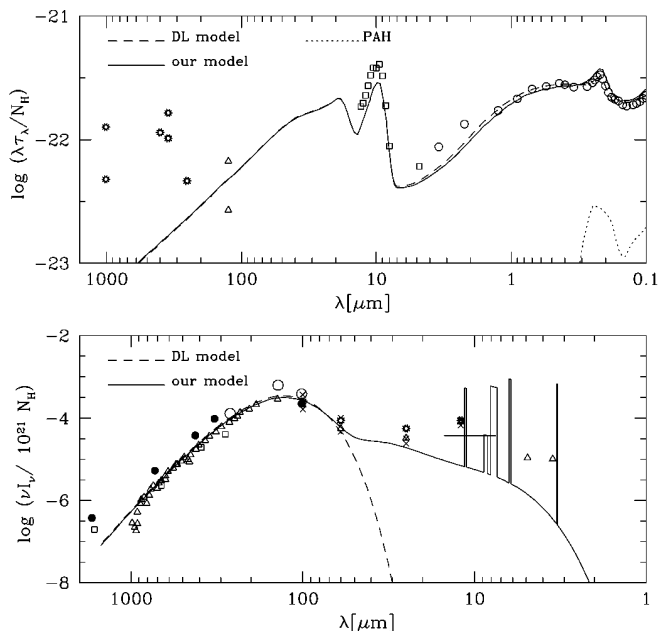


FIG. 3.—*Top*: Extinction curves of the dust model we adopt for diffuse and molecular gas, and that by Draine & Lee (1984) are compared with available data. *Bottom*: Predicted emissivity of grains ($\text{ergs s}^{-1} \text{cm}^{-2} \text{sr}^{-1} N_{\text{H}}^{-1}$) in the local interstellar radiation field (Mathis, Mezger, & Panagia 1983) compared with observations toward the galactic pole. The horizontal line around $12 \mu\text{m}$ marks the flux level obtained by convolving our expected SED with the $12 \mu\text{m}$ IRAS passband. *Bottom*: Triangles are data from Dwek et al. (1997), for references to other observations see Rowan-Robinson (1992, 1986).

to small grains. Actually using DL optical efficiencies, we find that the EUV part of the extinction curve is produced by small grains. Our σ_{PAH} rests on laboratory measurements and predicts, in the local interstellar radiation field, a PAH absorption and subsequent IR emission lower by a factor ~ 0.5 with respect to the Désert et al. (1990) analytical approximation.

In order to compute the IR emission of PAHs, their heat capacity $C_{\text{PAH}}(T)$ must be specified. A numerically convenient and accurate enough representation of the estimate given by Léger, d'Hendecourt, & Defourneau (1989a) is

$$\frac{C_{\text{PAH}}(T)}{C_{\text{max}}} = \begin{cases} 9.25 \times 10^{-4} T & \text{if } T < 800 \text{ K,} \\ 2 \times 10^{-4} T + 0.58 & \text{if } 800 \leq T < 2100 \text{ K,} \\ 1 & \text{if } T \geq 2100 \text{ K,} \end{cases} \quad (7)$$

where $C_{\text{max}} = 3(N_t - 2)k$ and $N_t = N_C + N_H$ is the total number of atoms (carbon and hydrogen) in the molecule. We adopt a population of PAHs with a distribution $dn/dN_C \propto N_C^{-2.25}$ from $N_C = 20$ to $N_C = 280$. Smaller molecules are easily destroyed by UV photons (Omont 1986). This distribution is quite similar to those adopted by other authors (Dwek et al. 1997; Désert et al. 1990). Astrophysical PAHs are thought to be partially *dehydrogenated*: probably owing to the large UV flux in the emission regions, some of the CH bonds, responsible for the 3.3, 8.6, and 11.3 μm bands, are broken. The number of H atoms in a molecule is thus written as $N_H = x_H N_{s,H}$, where $N_{s,H}$ is the number of hydrogen sites and x_H is the H coverage. The relationship between $N_{s,H}$ and N_C depends on the arrangements of hexagonal cycles in the molecule. The ratio $N_C/N_{s,H}$ is rather constant around 2 for laboratory PAHs molecules, for

which $N_C \lesssim 50$. However, the structure of typical interstellar PAHs is likely closer to that of *catacondensed* PAHs (Omont 1986), which are the most compact and stable ones and have the general formula $C_{6p^2}H_{6p}$, i.e., $N_{s,H} = (6N_C)^{0.5}$. For these quasi-circular molecules, usually assumed to represent the gross features of interstellar PAHs, the radius is given by $a = 0.9N_C^{1/2} \text{ \AA}$ if $N_C \gg 1$. With the above relationship between $N_{s,H}$ and N_C the typical flux ratios observed in the ISM between CH and CC bands (Mattila et al. 1996) is fairly well reproduced by our PAH model setting $x_H = 0.2$

PAHs emissivity was then computed following substantially the guidelines given by Xu & De Zotti (1989).² The adopted abundances of PAH molecules in the diffuse ISM and in the MCs implies that 18 and 1.8 ppm of C are locked in this component, respectively. Indeed there are indications showing that in denser environments and/or in stronger UV radiation field the relative number of small particles is significantly diminished (Puget & Léger 1989; Kim & Martin 1996, and references therein). In particular Xu & De Zotti (1989) concluded that PAH molecules are less abundant by a factor ~ 10 in our Galaxy star-forming regions than in the diffuse gas.

As apparent from Figure 3, this model reproduces reasonably well both the extinction from IR to UV and the whole cirrus emission. The model predicts an extinction below a few observational estimates at $\lambda \gtrsim 300 \mu\text{m}$ by a factor ~ 10 . To account for this, Rowan-Robinson (1986, 1992) introduced ad hoc modifications of the grain optical properties in his discretized models. We avoid in general this approach (but see § 3.1) mainly because these data have large uncertainties (DL), as it is apparent from their scatter. Moreover they refer to dusty environments for many respects different from the diffuse dust, which is instead the dominant contributor to the emission at $\lambda \gtrsim 100 \mu\text{m}$ in our galaxy models. Also it has been suggested that the silicate grain absorption in the submillimeter wavelength range may decline less steeply than λ^{-2} (Agladze et al. 1996).

The adopted mixture, even taking into account the contribution of PAH emission features, tends to underpredict the MIR cirrus emission, in particular the shorter λ data. A larger quantity of small grains and/or PAH molecules would improve the match with DIRBE observations, but would also produce a large disagreement with observed UV-extinction (Dwek et al. 1997). We prefer to adopt a compromise more balanced toward the extinction law, since in our models and in most interesting cases the MIR emission is in general dominated by warm dust in MCs rather than thermally fluctuating grains in the cirrus, whereas a good specification of the extinction properties is crucial. Moreover, DIRBE cirrus data at short wavelength could be affected by significant systematic effects (Dwek et al. 1997).

The total (i.e., cirrus + MCs) dust content of a galaxy ISM depends on the residual gas and on dust-to-gas ratio δ . The residual gas mass is provided at each time step by the chemical evolution model (see above). Determinations of δ in our Galaxy ISM and in nearby objects range typically from 1/100 to 1/400. For the purpose of this paper, where the model is compared only to galaxies in the local universe, we simply set $\delta = 1/110$, the standard value of DL model.

² Apart from two imprecisions in their equations: the factor 2 before σ_{PAH} in their eq. (13) is wrong since their cross section already takes into account the two molecule surfaces. On the other hand, the integration over solid angle yields a factor 4π before I_ν in the same equation, which in conclusion should be multiplied by a factor 2π on the right-hand side.

However, the code is thought to interpret data on objects in very different evolutionary stages; thus, we need in general a recipe to scale δ when the chemical conditions in the ISM are very different. We adopt the simplest assumption $\delta \propto Z$, with the proportionality constant adjusted to have $\delta = 1/110$ for $Z = Z_{\odot}$.

A recent difficulty for models relying on populations of carbon-based grains, the so-called *carbon crisis*, is connected with the quite uncertain determination of cosmic abundance of this element. Indeed these models were developed under the hypothesis that the measured solar system abundances (either in meteorites or solar photosphere) were also typical for the ISM. For instance DL, as well as our model, requires 282 ppM of C in grains, assuming a graphite density of 2.26 g cm^{-3} . This is 55% of the solar abundance that was adopted by DL as cosmic reference abundance (but $\sim 80\%$ of the more recent estimate in the solar system, $\simeq 365$ ppM quoted by Anders & Grevesse 1989). However in the last few years evidence has been accumulated that solar abundances may not be representative of the ISM. In particular in young star photospheres carbon is found to be only $\simeq 200\text{--}250$ ppM (e.g., Snow & Witt 1995, 1996; Gies & Lambert 1992). This, if really representative of the ISM abundance, would put restrictions difficult to meet by carbon-based dust models (Sofia, Cardelli, & Savage 1994; Cardelli et al. 1996; Mathis 1996), especially when taking into account that about 140 ppM seem to be in gas phase (Cardelli et al. 1996), leaving for dust only about $\frac{1}{3}$ of the C required by the DL model.

Possible ways out have been suggested: for instance big grains could be porous, likely because they are built up by the sticking of smaller ones (Mathis & Whiffen 1989; Mathis 1996), or dust could be to some extent prevented to be incorporated into stars during their formation (Snow & Witt 1996). Also the introduction of carbonaceous grains in a form other than graphitic (amorphous carbon, possibly hydrogenated, or composite grains), the use of more complex size distribution than a simple power law, and an elongated grain shape tend to alleviate the C requirements (Mathis 1996; Kim & Martin 1996).

Since these problems are still far from being clarified and our major concern is to obtain a good description of the absorption and emission properties of dust, we maintain by now a DL-type model, looking only for the minimum modifications required to obtain an acceptable overall match of the extinction curve from the UV to the far-IR and of the galactic cirrus emission. It is worth noticing that in the future this goal should be achieved with a more efficient use of the available cosmic carbon. The main effect of this on our spectrophotometric galaxy models will be a possible decrease of the required dust-to-gas ratio by a factor up to ~ 2 .

2.5. The Radiative Transfer in Dusty Media

As already remarked, to get the SED from 0.1 to 1000 μm , we have to solve the transfer equation for the radiation in presence of dust in the case of molecular clouds and diffuse ISM.

2.5.1. Radiation Transfer in MCs and Emerging Spectra

In the Galaxy virtually all the star formation activity resides in molecular clouds. Maps of CO and other tracers show that MCs are nonuniform, highly structured objects, containing density-enhanced regions, the cores, wherein

star formation (SF) actually occurs. This implies the clustering of young stars at different locations inside giant molecular clouds (GMCs), as confirmed by infrared imaging. The first evolutionary stages are hidden at optical wavelengths and a significant fraction, if not all, of the energy of young stellar objects is reprocessed by dust and radiated in the IR, only a minor fraction is reradiated as recombination lines. The powerful stellar winds and outflows and the ionizing flux from massive stars all contribute to the destruction of the molecular clouds in a timescale comparable to the lifetime of OB stars, $\sim 10^6\text{--}10^7$ yr. Thus, stars gradually get rid of their parent gas and become visible at optical wavelengths. The typical dust densities in these objects are so high that even IR photons are self-absorbed; thus, to compute the emitted SED the radiative transfer equation must be solved.

The complex evolution depicted above is simulated as follows. A fraction f_{mc} of the model gas mass M_{gas} at t_{G} is ascribed to the dense phase under discussion in this section. Recent estimates in our Galaxy suggest that half of the hydrogen mass is molecular H_2 , mainly in clouds with diameters $\gtrsim 10$ pc. The molecular gas $M_{\text{mc}} = f_{\text{mc}} M_{\text{gas}}$ is then subdivided into spherical clouds of assigned mass and radius, m_{mc} and r_{mc} , which may range in the typical observed intervals $\sim 10^5\text{--}10^6 M_{\odot}$ and $\sim 10\text{--}50$ pc, respectively. It is then supposed that each generation of stars, represented in our scheme by a SSP, is born within the cloud and progressively escapes it. This is mimicked by linearly decreasing the fraction f of SSP energy radiated inside the cloud with its age t :

$$f = \begin{cases} 1 & \text{if } t \leq t_0, \\ 2 - t/t_0 & \text{if } t_0 < t \leq 2t_0, \\ 0 & \text{if } t > 2t_0. \end{cases} \quad (8)$$

The model parameter t_0 introduced by this relation sets the fraction of starlight that can escape the starbursting region. The starlight locked up inside the cloud is approximated as a single central source. The cloud optical depth is fixed by the cloud mass and radius and by the dust-to-gas ratio. The emerging spectrum is obtained by solving the radiative transfer through the cloud with the code described by Granato & Danese (1994).

The distribution of stars in real GMCs implies a dust temperature distribution with many hot spots and cooler regions randomly distributed. A complete discussion of the effects of different approximations in this complex geometrical situation, including the single central source adopted here, can be found in Krügel & Siebenmorgen (1994, see in particular their Fig. 1a). An obvious drawback of our approach is an overestimate of the amount of very hot dust around the source, with respect to the more realistic approximation in which the stars are split in many sources at different locations. On the other hand, the approximation of a central point source is not much different from the IR spectrum predicted by a full treatment with hot spots, if the emission from the whole cloud is considered (Krügel & Siebenmorgen 1994).

Since the treatment of many hot spots in the cloud would introduce many other geometrical parameters and would slow down considerably our code due to the loss of symmetry, we simply treat the maximum temperature T_s of the grains at the inner edge as a parameter, summarizing in some way the geometrical parameters that would result in a

lower “true” maximum temperature: lowering the grain “sublimation” temperature produces a lower average temperature with a less opaque cloud. This brings the overall spectrum very close to that predicted with a proper treatment of the hot spots. It is, anyway, interesting to note that Gordon et al. (1997) found that their *shell geometry*, similar to that adopted here, is suited to explain the observed optical and UV properties of starburst galaxies, whereas the *dusty geometry*, in which dust and stars share the same spatial distribution, is not, even allowing for clumpiness.

For typical values of the relevant parameters our model predicts IR spectra of star-forming regions peaking around 40–60 μm (in a νL_ν plot), depending on the optical depth, with a rather steep decrease at longer wavelengths. We found that this behavior reproduces quite well the typical range of IR spectra of galactic YSOs, H II, and star-forming regions (e.g., Rowan-Robinson 1979; Ward-Thompson & Robson 1990; Men’shchikov & Henning 1996). For instance in Figure 4 the observed SED of W49A, a huge star-forming region composed of H II regions and giant molecular clouds, is compared with the spectrum of the MC component we use in the fit of the overall SED of Arp 220. Indeed we think that this ultraluminous infrared galaxy is a good benchmark for our MCs model, having an IR spectrum dominated by this component (see § 3.1).

2.5.2. Propagation in the Diffuse ISM and Cirrus Emission

Before escaping the galaxy the light arising from stellar populations and from molecular clouds interacts with the diffuse dust component.

We adopt a simplified treatment of radiative transfer in the diffuse gas that ignores dust self-absorption and approximates the effects of optical-UV scattering by means of an effective optical depth, given by the geometrical mean of the absorption and scattering efficiencies $\tau_{\text{eff}}^2 = \tau_a(\tau_a + \tau_s)$ (Rybicky & Lightman 1979, p. 36). Indeed the relatively low opacity of dust in the IR regime, where the dust emission

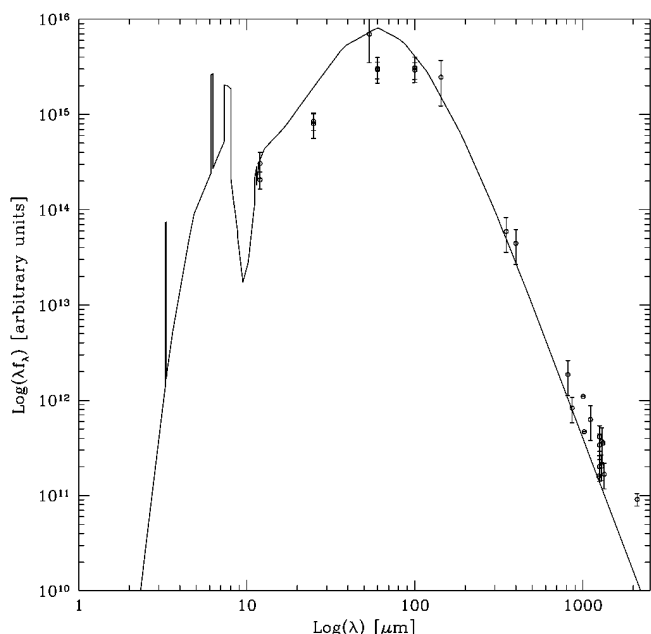


FIG. 4.—Observed SED of W49A (Ward-Thompson & Robson 1990), a huge star-forming region composed of H II regions and GMCs, is compared with the spectrum of the MC component we use in the fit of the overall SED of Arp 220.

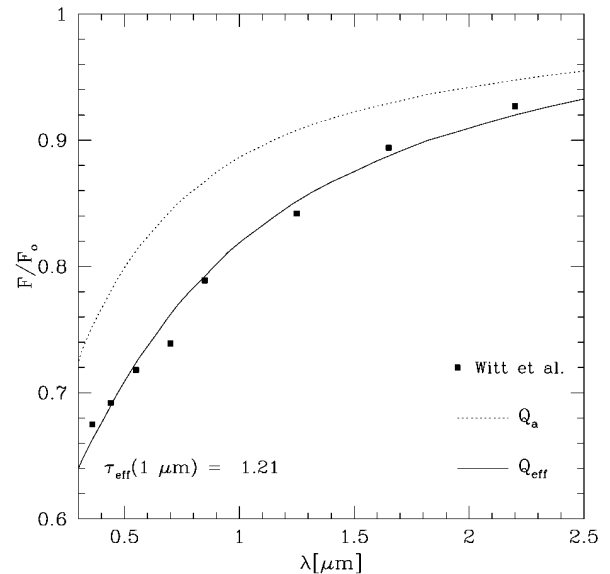


FIG. 5.— F/F_0 is the ratio between the dust extinguished flux and that expected if dust were not present. The points have been computed by Witt et al. (1992) with a Monte Carlo radiative transfer code including anisotropic scattering, the dashed line represents the result of our code taking into account only absorption, whereas the solid line includes scattering with the effective optical depth $\tau_{\text{eff}}^2 = \tau_a(\tau_a + \tau_s)$. The adopted geometry is that defined by Witt et al. (1992) as *elliptical galaxy*.

occurs, implies that in most cases of interest the diffuse ISM is transparent to its own photons. Our approximation for combined scattering and absorption processes is rigorously applicable only to an infinite homogeneous medium and isotropic scattering. However we checked, by comparing our results with those obtained by Witt et al. (1992) by means of a Monte Carlo radiative transfer code including anisotropic scattering, that it is fairly good in most “real-world” geometrical arrangements (see Fig. 5).

The galaxy is subdivided into small volume elements V_i . The local (angle averaged) radiation field in the i th element due to the extinguished emissions of free stars and MCs from all the elements is computed from

$$J_{\lambda,i} = \sum_k \frac{V_k(j_{\lambda,k}^{\text{mc}} + j_{\lambda,k}^*) \exp[-\tau_{\text{eff},\lambda}(i,k)]}{r^2(i,k)}, \quad (9)$$

where $\tau_{\text{eff},\lambda}(i,k)$ and $r(i,k)$ are the effective optical thickness and the distance between the elements i and k , respectively. Then the local dust emissivity is calculated as described in § 2.4. Finally the specific flux measured by an external observer in a given direction θ is derived as a sum over the galaxy of the extinguished emissivity of free stars, MCs, and diffuse dust:

$$F_\lambda(\theta) = 4\pi \sum_k V_k j_{\lambda,k} \exp[-\tau_{\text{eff},\lambda}(k,\theta)], \quad (10)$$

where $\tau_{\text{eff},\lambda}(k,\theta)$ is the optical thickness from the element k to the outskirts of the galaxy along the direction θ .

In the code the spheroidal systems are assumed to extend up to the tidal radius $r_t = 10^{2.2} r_c$ (of the star component), whereas exponential disks are truncated at $6R_d$, where R_d is the largest of the three components. Since more than 98% of the mass is included within these radii, adoption of larger cutoff radii would not produce any significant difference. Deviations from the energy balance between dust emission and absorption, which mainly depend on the number of

volume elements in which the galaxy is subdivided, are kept within less than 2%–5%.

3. COMPARISON WITH THE DATA

A few examples, which show the capability of our model to reproduce the data on starbursting and normal galaxies in the local universe, are discussed below. We restrict ourselves to galaxies for which available photometric observations allow a precise evaluation of the SED for UV to far-IR. The fitting parameters are reported in Tables 1 and 2 for the chemical model (step 1) and for the photometric model (step 2), respectively. Table 3 summarizes a few rele-

vant quantities derived from those parameters. Since the purpose of this paper is to present a procedure to take into account the radiative effects of the ISM, the parameters t_{inf} and ν (Table 1), which rule the SF history of the galaxy, were set following the general results of papers dealing with the chemical evolution of different types of galaxies (see Matteucci 1996 for a review), under the major constraint of getting a suitable amount of residual gas. The following parameters have been fixed to reasonable values: galactic age $t_G = 13$ Gyr, dust-to-gas mass ratio $\delta = 9 \times 10^{-3}$, exponent of Schimdt SFR $k = 1$, maximum temperature of dust in MCs $T_s = 400$ K, mass of single MC $m_{\text{mc}} = 10^6 M_\odot$.

TABLE 1
STAR FORMATION HISTORY PARAMETERS

Object (1)	D Mpc (2)	M_G ($10^{10} M_\odot$) (3)	ν (Gyr^{-1}) (4)	t_{inf} (Gyr) (5)	M_{burst} ($10^{10} M_\odot$) (6)	t_{burst} (Gyr) (7)	t_e (Gyr) (8)
M82.....	3.25	1.8	1.2	9	0.02	12.95	0.05
NGC 6090	175	41	0.6	9	0.16	12.95	0.05
ARP 220	115	23	0.3	9	2.5	12.95	0.05
M51.....	9.6	15.5	0.6	4
M100	20	20	0.75	4
NGC 6946	6.7	12.5	0.6	5
Giant elliptical.....	...	100	2.0	0.1

NOTE.—Parameters for the star formation history (§ 2.1): col. (2) adopted distance; col. (3) final baryonic galaxy mass; col. (4) SF efficiency; col. (5) infall timescale; col. (6) gas mass converted into stars during the burst; col. (7) galaxy age at beginning of the burst (when included); col. (8) e -folding time for SFR in the burst. All models have an age of 13 Gyr. In the case of the giant elliptical the SF has been stopped at 1.15 Gyr.

TABLE 2
GEOMETRIC PARAMETERS

Object (1)	f_{mc} (2)	r_{mc} (pc) (3)	t_0 (Myr) (4)	r_c^* (kpc) (5)	r_c^c (kpc) (6)	R_d (kpc) (7)	z_d (kpc) (8)
M82.....	0.08	16	57	0.15	0.2
NGC 6090	0.005	17	18	0.5	1.0
ARP 220	0.5	10.6	50	0.5	0.5
M51.....	0.7	14	8	4.7	0.4
M100	0.8	15	3	5.0	0.4
NGC 6946	0.6	14	2.5	8.0	1.0
Giant elliptical.....	0.4	6.0

NOTE.—Parameters for the photometric model estimated from SED fitting: col. (2) fraction of residual gas in MCs; col. (3) radius of MC; col. (4) parameter regulating the escape of young stars from MCs (eq. [8]); cols. (5)–(8) parameters for the spatial distribution of stars, MCs, and cirrus (eqs. [1] and [3]). For disks the inclination angles have been taken from the literature (see text) and are $i = 20^\circ$ (M51), $i = 30^\circ$ (M100), and $i = 34^\circ$ (NGC 6946).

TABLE 3
DERIVED QUANTITIES

Object (1)	$\langle \text{SFR} \rangle$ ($M_\odot \text{ yr}^{-1}$) (2)	M_{dust} ($10^7 M_\odot$) (3)	τ_1^{mc} (4)	$\bar{\tau}_1$ (5)	$\bar{\tau}_B$ (6)	L_{mc} ($10^{44} \text{ ergs s}^{-1}$) (7)	L_c ($10^{44} \text{ ergs s}^{-1}$) (8)	$L_{\text{Ly}\alpha}$ ($10^{44} \text{ ergs s}^{-1}$) (9)
M82.....	5.5	0.8	25	0.62	1.30	1.1	0.25	0.09
NGC 6090	68	45	24	0.84	1.37	13	13	1.3
ARP 220	580	30	58	1.67	2.80	100	5.7	8.7
M51.....	6	10.4	33	0.06	0.28	1.01	0.90	0.11
M100	7	9.6	29	0.03	0.15	0.84	0.85	0.12
NGC 6946	6	10.4	33	0.03	0.12	0.62	0.53	0.10
Giant elliptical.....	...	0.15	...	0.00	0.01	...	0.02	0.03

NOTE.—A few quantities derived from the models: col. (2) SFR averaged over the last 5×10^7 yr, which is the time from burst onset for starburst models; col. (3) total mass in dust in the galaxy; col. (4) $1 \mu\text{m}$ optical thickness of the MCs from the center; col. (5) $1 \mu\text{m}$ “average” optical thickness of the model, defined such as [observed flux] = [dust-free flux $\times \exp(-\bar{\tau})$]; col. (6) same as col. (5) but at $0.44 \mu\text{m}$; col. (7) luminosity of the MCs; col. (8) luminosity of the diffuse dust; and col. (10) luminosity in the Lyman continuum *before dust absorption*.

Moreover the mass limits of the Salpeter IMF are the standard $M_{\text{up}} = 100 M_{\odot}$ and $M_{\text{low}} = 0.1$, but for starburst galaxies the estimates of dynamical mass require $M_{\text{low}} \gtrsim 0.2$, as discussed below. We also remind the reader that, in order to keep the number of free parameters to the minimum required by present quality data, we set the scale lengths of stars and gas distributions in spirals to the same values, i.e., $R_d^* = R_d^c$ and $z_d^* = z_d^c$.

As previously noticed, the SED of the MC component is set mainly by its optical depth (Table 3) $\propto m_{\text{mc}}/r_{\text{mc}}^2$, which is in some sense the true “fitting parameter” for this component (together with t_0), rather than r_{mc} reported in Table 2. In other words the values found for r_{mc} depend on having set $m_{\text{mc}} = 10^6 M_{\odot}$, as typical for giant molecular clouds in the Galaxy, and r_{mc} could well be varied by a factor ~ 2 , producing almost equivalent fits, provided m_{mc} is adjusted to keep $m_{\text{mc}}/r_{\text{mc}}^2$ constant.

3.1. Starburst Galaxies

3.1.1. M82

In the prototype starburst galaxy M82 the burst was probably triggered by the interaction with M81, some 10^8 yr ago (Solinger, Morrison, & Markert 1977). Thanks to the proximity of this system ($D = 3.25$ Mpc) a wealth of data do exist, providing a well-sampled full coverage of the SED at different angular resolutions, as well as other observational constraints. The fit (Fig. 6) is obtained by evolving for 13 Gyr an open system with a final baryonic mass of $1.8 \times 10^{10} M_{\odot}$, a factor 6 less than the estimated total dynamical mass (Doane & Mathews 1993). We adopted $M_l = 0.2 M_{\odot}$ as lower limit of the Salpeter IMF. A lower value would require a baryonic mass closer to the dynamical mass. The assumed parameters provide a SFR raising from 0 to about $3 M_{\odot} \text{ yr}^{-1}$ in the first 3 Gyr, then smoothly declining to $1.35 M_{\odot} \text{ yr}^{-1}$ at $t = 13$ Gyr. To this gentle star formation history, which leaves a gas fraction of 0.064, we have superposed an exponential burst processing 18% of the residual gas in the last 5×10^7 yr, with an e -folding time also of 5×10^7 yr (Fig. 7). Note that our results are almost independent on the precise evolution of the SFR in the

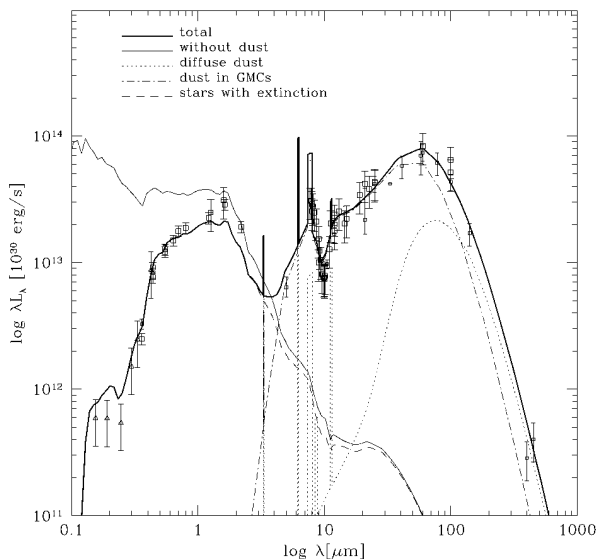


FIG. 6.—Fit to the SED of M82. Data are from Code & Welch (1982), Soifer et al. (1987), Klein, Wiebeinski, & Morsi (1988), Cohen & Volk (1989), van Driel et al. (1993), Ichicawa et al. (1994, 1995).

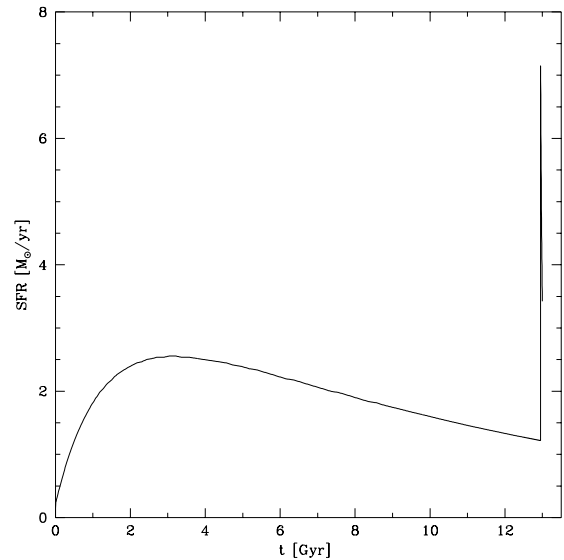


FIG. 7.—M82: SFR as a function of galactic time

burst: even a constant burst yields very similar estimates of the relevant quantities. Also the duration of the burst could be doubled or halved with small adjustment of the other parameters without damaging the quality of the SED fit. Thus we end with a total gas mass of $8.6 \times 10^8 M_{\odot}$, 8% of which is ascribed to the molecular component, organized in clouds with $m_{\text{mc}} = 10^6 M_{\odot}$ and $r_{\text{mc}} = 16$ pc. These clouds reprocess almost completely the starlight due to the burst. The system is assumed to follow a King profile with $r_c^* = 150$ pc for stars and $r_c^c = 200$ for diffuse gas.

The masses we ascribe to the various components favorably compare with radio estimates of total gas masses $\sim 10^9 M_{\odot}$ (Solinger et al. 1977), with CO determinations of gas in molecular form $\sim 10^8 M_{\odot}$ (Lo et al. 1987; Wild et al. 1992), and with an upper limit $\lesssim 3 \times 10^8 M_{\odot}$ to the mass of stars formed in the burst, suggested by dynamical considerations (McLeod et al. 1993). Also, in our proposed model the predicted supernova rate (SNR) is between 0.05 and 0.1 yr^{-1} , depending on the adopted lower limit of stellar mass yielding to supernova (SN) explosion 9 or $6 M_{\odot}$, respectively. Observational estimates suggest a SNR in the range 0.07– 0.3 yr^{-1} (McLeod et al. 1993; Doane & Mathews 1993). Increasing the lower limit of the IMF in the burst to, for instance, $M_l = 1.0 M_{\odot}$ would increase the SNR by a factor ~ 2 . In conclusion the model required to nicely reproduce the observed SED turns out to be in agreement with independent estimates of masses and of SNR.

3.1.2. NGC 6090

This strongly interacting galaxy at 175 Mpc ($H_0 = 50 \text{ km s}^{-1} \text{ Mpc}^{-1}$) has been observed by *ISO* from 2.5 to $200 \mu\text{m}$ (Acosta-Pulido et al. 1996). The SED resulting from the combination of these data with previously published optical photometry is nicely reproduced by our model (Fig. 8). The differences in the parameters with respect to M82, apart from an up scale in involved baryonic mass ($4.1 \times 10^{11} M_{\odot}$), are aimed at enhancing the diffuse dust emission at $\lambda \gtrsim 100 \mu\text{m}$, which, as noticed by Acosta-Pulido et al. (1996), is not reproduced by published starburst models. Thus the preburst SFR has been adjusted to leave a larger gas fraction (0.127), 3.2% of which is processed by the burst.

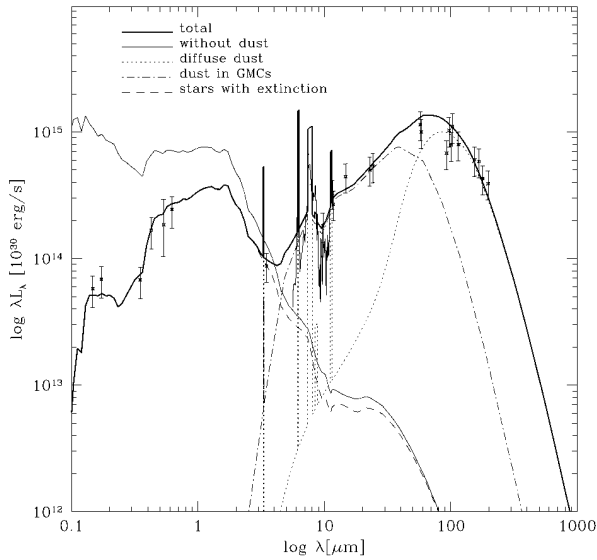


FIG. 8.—Fit to the SED of NGC 6090. Data are from Mazzarella & Boroson (1993), Acosta-Pulido et al. (1996), Gordon et al. (1997).

The molecular star-forming clouds account only for 0.5% of the gas left by the burst.

3.1.3. Arp 220

Arp 220 is an archetypal ultraluminous infrared galaxy (ULIRG), most likely the result of a recent merging between two gas-rich galaxies, for which ISOPHOT data have been now published (Klaas et al. 1997), and whose K -band light profile resembles that of a typical elliptical galaxy. In this object there is evidence of both starburst, as well as Seyfert, activity, but *ISO* spectroscopy led to the conclusion that the IR luminosity is primarily ($\gtrsim 90\%$) powered by starburst (Sturm et al. 1996). The fitting model requires a strong burst, converting into stars $2.5 \times 10^{10} M_{\odot}$, i.e., as much as 11% of the total baryonic mass, and a high fraction 50% of residual gas in star-forming clouds. The gas fraction before the burst is 0.25. As a result, the IR and submillimetric emission is everywhere dominated by dust associated with star-forming regions. The mass in molecular gas is $\sim 1.6 \times 10^{10} M_{\odot}$, in agreement with CO estimates (Solomon et al. 1997; Scoville, Yun, & Bryant 1997). From a determination of the CO rotation curve Scoville et al. (1997) infer a dynamical mass of $\sim 3\text{--}6 \times 10^{10} M_{\odot}$ within $r \simeq 1.5$ kpc (depending on the adopted potential), in agreement with the mass requested by our model within the same radius $\simeq 4.1 \times 10^{10} M_{\odot}$.

We find that the submillimetric data of Arp 220 are underpredicted by a factor $\sim 2\text{--}3$ by any model that successfully reproduces the remaining SED, unless the long wavelength decline of grain absorption efficiency is reduced, say from $\propto \lambda^{-2}$ to $\propto \lambda^{-1.6}$ above $\simeq 100 \mu\text{m}$ (see Agladze et al. 1996 for laboratory measurements supporting this possibility for silicate grains). In Figure 9 we report fits obtained adopting either the modified, as well as the standard, DL cross sections.

3.2. Normal Galaxies

In the following we examine objects that do not show clear signs of enhanced SF or nuclear activities in the SED or in the morphology, namely, three late-type spirals and a giant elliptical template. Indeed elliptical galaxies form a

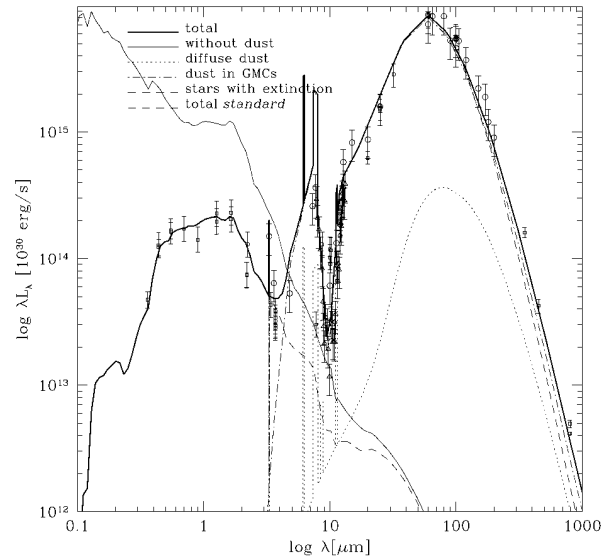


FIG. 9.—Arp 220: in this case the wavelength dependence of grain cross section has been modified above $100 \mu\text{m}$ from $\propto \lambda^{-2}$ to $\propto \lambda^{-1.6}$. The dashed line above $100 \mu\text{m}$ represents the model prediction with standard λ^{-2} decline. Data are from Carico et al. (1988), Sanders et al. (1988), Smith, Aitken, & Roche (1989), Carico et al. (1990), Wynn-Williams & Becklin (1993), Rigopoulou, Lawrence, & Rowan-Robinson (1996), Klaas et al. (1997).

relatively homogeneous class, whereas this is not the case for spirals. We fitted spirals later than Sb, which are clearly disk-dominated, and we adopt for them an exponential geometry (see § 2.3).

3.2.1. M51

In Figure 10 we present a fit to the SED of the nearly face-on ($i = 20^\circ$; Tully 1974) Sbc galaxy M51 (NGC 5194), taken at a distance $D = 9.6$ Mpc (Sandage & Tammann 1975). Since the discrepancy between *ISO* and *IRAS* data at 60 and $100 \mu\text{m}$ could be due to an excess of the *ISO* point-spread function (Hippelein et al. 1996), we fitted the *IRAS*

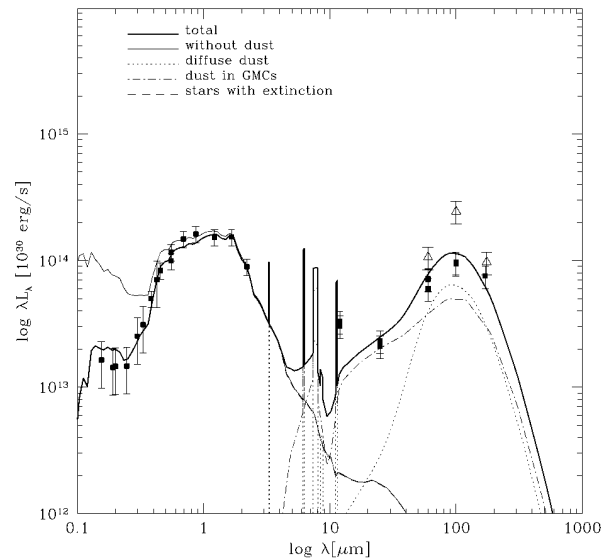


FIG. 10.—Fit to the SED of the Sbc galaxy M51. Data are from Buat, Deharveng, & Donas (1989), Evans (1995), de Vaucouleurs et al. (1991) Third Reference Catalog of Bright Galaxies (RC3), Code & Welch (1982), Young et al. (1989), Rice et al. (1988), Devereux & Young (1990, 1992), Smith (1982), Hippelein et al. (1996) (*ISO*, triangles).

data. The model has a baryonic mass of $1.55 \times 10^{11} M_{\odot}$, whose evolution leaves at 13 Gyr a gas fraction of 0.067, 70% of which is in molecular form. The mass of ISM in the molecular and diffuse components, as well as their relative fraction, is in agreement within a factor ≤ 2 , with estimates by Scoville & Young (1983), Young et al. (1989), and Devereux & Young (1990). Gas and stars are exponentially distributed with the same scale lengths, 4.7 and 0.4 kpc for the radial and vertical scales, respectively. The former value is in good agreement with those estimated by Beckman et al. (1996) from observed brightness distributions in different optical bands. Owing to the low energy output observed at $\lambda \lesssim 0.2 \mu\text{m}$, stars born during the last 5×10^6 yr are hidden inside molecular clouds.

The striking correspondence between the $15 \mu\text{m}$ emission mapped by ISOCAM and the $\text{H}\alpha$ emission indicates that the MIR is powered by recent star formation (Sauvage et al. 1996). As for the far-IR (FIR), somewhat contradictory claims have been reported: Devereux & Young (1992), comparing the radial distributions of FIR, $\text{H}\alpha$, H I , and H_2 emission, concluded that the same holds true in the range 40–1000 μm , whereas Hippelein et al. (1996) found no obvious correlation between FIR ISOPHOT maps and $\text{H}\alpha$ fluxes. This apparently complex situation is not surprising, since according to the model the MIR emission is provided by the MC component, whereas above $\sim 60 \mu\text{m}$ the diffuse dust gives a comparable contribution, which, however, is in part powered by young stars.

3.2.2. M100

The Sbc galaxy M100 (NGC 4321) is the largest spiral in the Virgo Cluster. We adopt a distance $D = 20$ Mpc and an inclination angle $i = 30^\circ$. The model in Figure 11 has a baryonic mass of $2 \times 10^{11} M_{\odot}$, with a residual gas fraction of 0.048, 80% in molecular form. Indeed, according to the gas masses estimated by Young et al. (1989) and Devereux & Young (1990), which are larger than ours by a factor $\simeq 2$, the ISM seems to be dominated by the molecular component. The location of M100 in the central regions of the Virgo Cluster could affect some of its properties, as the H I

distribution that shows a sharp edge in correspondence to the optical radius (Knapen et al. 1993). This could be the reason for the warm FIR SED observed in M100, as compared to M51 and NGC 6946, despite their morphological similarity. The steep decline of the spectrum in the submillimeter region has been interpreted by Stark et al. (1989) as an indication that the emitting grains are warm and small. In our model this is not required since the fit is obtained with standard diffuse dust. Stars and dust share the same radial and vertical scale lengths, 5 and 0.4 kpc, respectively, in agreement with the values derived by Beckman et al. (1996) for the stellar component and with the H I distribution.

3.2.3. NGC 6946

The fit to this Scd galaxy at distance $D = 6.72$ Mpc (Rice et al. 1988) and inclination angle $i = 34^\circ$ (Considere & Athanassoula 1988), is shown in Figure 12. The total gas mass in the model, $1.04 \times 10^{10} M_{\odot}$, i.e., 8.3% of the baryonic mass, agrees with the molecular plus neutral hydrogen mass given by Young et al. (1989) or Devereux & Young (1990) (reported at 6.72 Mpc), whereas the fraction we ascribe to the molecular component is a factor $\simeq 2$ higher.

The contribution of young and old stellar populations to dust heating in this object has been considered by several authors. Devereux & Young (1993), comparing the radial distributions of FIR, $\text{H}\alpha$, H I , and H_2 , conclude that the 40 to 1000 μm luminosity is dominated by dust associated with molecular gas heated by young stars. However, *ISO* data reported by Tuffs et al. (1996) reveal an extended FIR emission out to a radius of $8'$, with a scale length similar to the *R*-band one, whereas little $\text{H}\alpha$ emission has been detected beyond $r \sim 6'$. This suggests that part of the observed cold FIR SED of NGC 6946 could be due to dust associated with a diffuse H I gas, which indeed extends out to $r \sim 15'$ (Boulanger & Viallefond 1992) and is heated mainly by old stellar populations. Malhotra et al. (1996) find that the radial scale lengths at 7 and 15 μm are similar to those in $\text{H}\alpha$ and H_2 but much shorter than those in *R*-band and H I , consistent with a warm dust emission primarily heated by

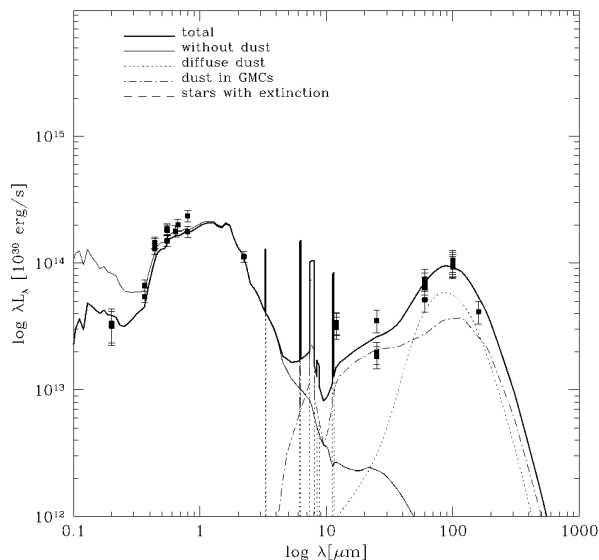


FIG. 11.—Fit to the SED of the Sbc galaxy M100. Data are from Buat et al. (1989), Donas et al. (1987), de Jong & van der Kruit (1994), Stark et al. (1989), RC3, Devereux & Young (1990), Young et al. (1989), Helou et al. (1988), Knapp, Helou, & Stark (1987).

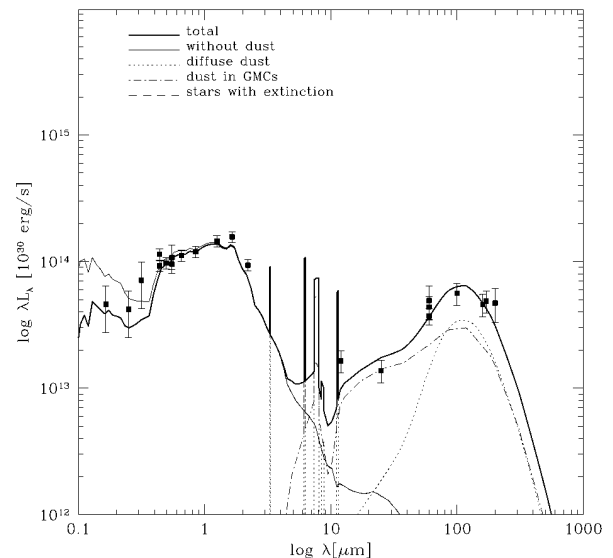


FIG. 12.—Fit to SED of the Scd galaxy NGC 6946. Data are from Rifatto, Longo, & Capaccioli (1995), RC3, Engargiola (1991), Devereux & Young (1993), Rice et al. (1988), Tuffs et al. (1996).

young massive stars. In the proposed fit the MIR emission arises from MC dust heated by newly born stars. The SED above $\sim 60 \mu\text{m}$ is almost equally contributed by MCs and diffuse dust, but, since $t_0 = 2.5 \text{ Myr}$, even the latter is predominantly heated by young stars.

Tacconi & Young (1986) estimate a scale length of 9.6 kpc for the cold ISM component, whereas for the star distribution their values range from 4 to 8 kpc, depending on the band and on the galactic component (disk or arms) considered. The model scale lengths are set to 8 kpc for both stars and the diffuse gas. The vertical scale lengths are 1 kpc to keep the diffuse dust emission sufficiently cold.

3.2.4. Giant Ellipticals

Ellipticals constitute a class of objects with fairly homogeneous spectral properties. It is then interesting to test our model against an average SED of giant elliptical galaxies, constructed combining the Arimoto's (1996) template from 0.12 to $2.2 \mu\text{m}$ with the median *IRAS* over *B* band fluxes of bright ellipticals estimated by Mazzei et al. (1994) and the average (K-L) color computed by Impey, Wynn-Williams, & Becklin (1986) (Fig. 13). The fit has been obtained with a "classical" star formation history model for ellipticals: an open model with infall and galactic wind. The high efficiency $\nu = 2$ causes a huge SFR in the first 1.2 Gyr interrupted by the onset of the galactic wind (see Tantaló et al. 1996 for a discussion of these values). The object is observed at 13 Gyr, when a comparatively very small fraction of galactic mass in a diffuse dusty component is sufficient to produce the observed *IRAS* emission. Note that this gas is not provided by the chemical model, according to which the bulk of the ISM is ejected by the galactic wind that stops the star formation. Thus in this case the mass in the diffuse dust $1.5 \times 10^7 M_\odot$ is a fitting parameter of our photometric model. This dusty ISM could arise from evolved stars of the passively evolving galaxy, by cooling flows or by merging activity. It is also worth noticing that r_c needs to be much greater for the ISM than for stars (6 and 0.4 kpc, respectively): for smaller values of r_c^c the cirrus emission would be too warm because dust would be more concentrated in the central regions where the radiation field is higher. Other authors already suggested that diffuse dust in

elliptical galaxies needs to be less concentrated than stars, on the basis of either optical color gradients (e.g., Wise & Silva 1996) or *IRAS* colors (e.g., Tsai & Mathews 1996). As discussed in § 2.5.2, an alternative proposed way to describe this lower concentration is to adopt the same r_c for both stars and diffuse dust, decreasing the exponent $\gamma = 1.5$ in the King law of stars. However for this SED, adjusting γ^c and r_c with the constraint $r_c^c = r_c^*$, we found only marginally acceptable fits in the *IRAS* regime, significantly worse than that presented in Figure 13.

4. DISCUSSION

When reproducing starburst galaxies, our model is characterized by the variations of six parameters related to the total mass and star formation history and of five geometrical parameters (Tables 1 and 2). For normal disk galaxies, the parameters become three and five, respectively. In order to fit the elliptical galaxy template, seven parameters have been adjusted, including the epoch at which the SF activity is stopped.

The masses reasonably constrained by matching the SED are the baryonic mass (although dependent on the IMF, particularly its lower limit) mostly from the energy emitted in the near-IR (NIR) by the old stellar component, and the mass of dust, from its MIR-FIR emission. Therefore the mass of gas present in the galaxy is constrained from the fit, provided δ is known. Our assumption $\delta = 9 \times 10^{-3}$ is likely the best guess for our Galaxy; however, in different systems and in the Galaxy itself, variations of a factor of a few are commonly quoted, e.g., Rand, Kulkarni, & Rice (1992) for M51 or Tuffs et al. (1996) for NGC 6946. As a consequence, our estimated gas masses suffer by a similar uncertainty. The SFR history of the old stellar component is constrained by the spectrum and, for starburst galaxies, also by the requirement that a certain amount of gas is available for the latest burst. The three analyzed starbursts exhibit rather different star formation histories, with the average SFR of the old component inversely proportional to the strength of the SFR in the burst. Estimates of masses in stars and gas, as well as of SF and SN rates from observations other than broadband spectra, discussed in the previous sections and below, nicely agree with those provided by our SED fitting.

4.1. Starbursts and ULIRGs

The SFR in a starbursting region can be estimated on the basis of the FIR luminosity, under the assumption that dust reradiates the overall bolometric luminosity and after calibration with stellar synthesis models. Kennicutt (1998) proposes $\text{SFR}(M_\odot \text{ yr}^{-1}) = L_{\text{FIR}}/(2.2 \times 10^{43} \text{ ergs s}^{-1})$, with calibration derived from models of Leitherer & Heckman (1995). This relationship properly applies to star-forming regions, whereas the extension to a galaxy as a whole is dangerous, since a nonnegligible portion of the FIR luminosity may arise from cirrus emission powered also by relatively old stars. However our model accurately determines the warm component associated to the MCs where star formation is occurring (L_{mc} in Table 3). For M82 our fit predicts an overall FIR luminosity associated to the MCs component of $1.1 \times 10^{44} \text{ ergs s}^{-1}$, which, following Kennicutt, translates in $\text{SFR} = 5.0 M_\odot \text{ yr}^{-1}$. Similarly, the SFRs inferred from the luminosity of the warm component is $57 M_\odot \text{ yr}^{-1}$ and $460 M_\odot \text{ yr}^{-1}$ for NGC 6090 and Arp 220, respectively. These figures are in very good agreement

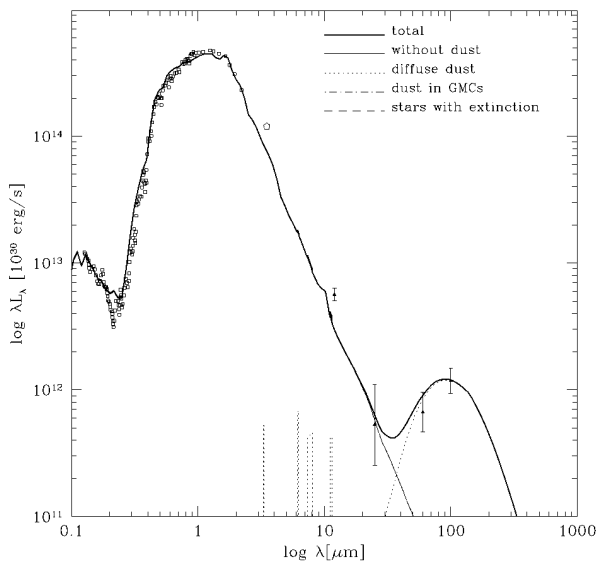


FIG. 13.—Fit to a template SED of a giant elliptical galaxy

with those derived by fitting the SEDs and reported in Table 3. Thus, whereas Kennicutt's calibration is confirmed, we stress that this refers only to the warm component, which contributes $\simeq 50\%$ of L_{FIR} in NGC 6090. This source of uncertainty adds to the obvious effect of the adopted IMF in the conversion from observed IR luminosity to SFRs.

Although the very recent (say in the last 10 Myr) SFR is relatively well constrained by the observed warm IR emission, the burst duration, and therefore the total mass converted into stars, can be varied within a factor ~ 2 , still yielding the correct L_{FIR} and spectra after readjustments of other parameters. However the supernova rates deduced from observations put further constraints on the average SFR and duration of the burst. In the well-studied case of M82 the model predicts a SN rate in the interval deduced by observations.

The SFR can also be inferred from the ionizing luminosity $L_{\text{Ly}\alpha}$, which can be derived from recombination lines. With the adopted IMF we find $L_{\text{Ly}\alpha}(10^{44} \text{ ergs s}^{-1}) \simeq 0.017 \text{ SFR}(M_{\odot} \text{ yr}^{-1})$, which holds with very small deviations for the six studied star-forming galaxies (see Table 3). The uncertainties connected to extinction corrections of observed line fluxes are minimized employing transitions occurring in the IR regime, such as Br γ line ($\lambda = 2.17 \mu\text{m}$). Calzetti (1997) and Kennicutt (1998), using Leitherer & Heckmann (1995) results, find $\text{SFR}(M_{\odot} \text{ yr}^{-1}) = L(\text{Br}\gamma)/1.6 \times 10^{39} \text{ ergs s}^{-1}$ by adopting a Salpeter IMF within $0.1\text{--}100 M_{\odot}$ or $\text{SFR}(M_{\odot} \text{ yr}^{-1}) = L(\text{Br}\gamma)/3.7 \times 10^{38} \text{ ergs s}^{-1}$ when the mass range is $0.1\text{--}30 M_{\odot}$.

The (Br γ) line luminosity $L(\text{Br}\gamma) = 9.2 \times 10^{40} \text{ ergs s}^{-1}$ of NGC 6090 (Calzetti, Kinney, & Storchi-Bergmann 1996) corresponds to a SFR = $56 M_{\odot} \text{ yr}^{-1}$ with the assumption of the $0.1\text{--}100 M_{\odot}$ mass range, only 18% less than that used in our model, whereas the smaller range in the IMF would predict a SFR higher by a factor 4. Kennicutt (1998) has shown that there is a clear trend for SFRs derived from L_{FIR} to be larger than those estimated from the $L(\text{Br}\gamma)$, suggesting that extinction is nonnegligible even at near-IR wavelengths.

Genzel et al. (1998) reported the ratio of the far-IR to Lyman continuum luminosity $L_{\text{FIR}}/L_{\text{Ly}\alpha}$ of starbursts (including M82) and ULIRGs, derived from near and mid-IR recombination lines. For 12 starburst galaxies the median value is $L_{\text{FIR}}/L_{\text{Ly}\alpha} \simeq 16$. The model ratio depends on the adopted IMF. Our fit to M82 overall SED yields $L_{\text{FIR}}/L_{\text{Ly}\alpha} \simeq 12$, where $L_{\text{Ly}\alpha}$ is the unextinguished luminosity of the (young) stellar populations below 912\AA in very good agreement with the value found by Genzel et al. (1998). For NGC 6090 the fit predicts $L_{\text{FIR}}/L_{\text{Ly}\alpha} \simeq 10$, using L_{mc} to evaluate the model L_{FIR} powered by the burst, well within the range of the values inferred by the same authors. As for Arp 220, which properly belongs to the ULIRG class, higher values $15 \lesssim L_{\text{FIR}}/L_{\text{Ly}\alpha} \lesssim 112$ are inferred from IR recombination lines, whereas our model predicts $L_{\text{FIR}}/L_{\text{Ly}\alpha} \simeq 11$. The discrepancy is likely due to the uncertain large correction for IR extinction in this object. Actually Genzel et al. (1998) use a screen obscuration with $A_V = 45$, whereas we find $A_V \simeq 150$ in MCs of this object. Interestingly enough, the 15 ULIRGs (including Arp 220) studied by Genzel et al. (1998) exhibit a median $L_{\text{FIR}}/L_{\text{Ly}\alpha} \simeq 40$, larger by a factor of ~ 2.5 than that inferred for starburst galaxies. This result can be explained by larger obscurations or by a softer intrinsic Lyman continuum, pointing to an

IMF less rich in massive stars or to an older starburst. In the models we used bursts that began 0.05 Gyr ago but are still rather active due to the large e -folding time $t_e = 0.05$ Gyr.

It is worth noticing that our model does not account for the ionizing radiation converted into recombination lines, which are much less absorbed by dust than the Lyman continuum. In the present version of the code the UV radiation can be only converted directly to IR photons through dust absorption. However the energy budget is not significantly affected, since the observed luminosity in recombination lines is only a few percent of the bolometric luminosity of starburst galaxies (e.g., Genzel et al. 1998).

The observed UV emission at $\lambda \gtrsim 1000 \text{\AA}$ is crucial in determining the fraction of the SSPs that escaped from the parent molecular clouds. In our model the UV flux emerging from a single galaxy depends on the age t_0 after which a SSP starts to get out from the molecular cloud. The UV photons are affected also by absorption in the diffuse ISM. In the case of M82 and Arp 220 the measured UV flux is a tiny fraction of the bolometric luminosity (see Figs. 6 and 9). This implies that the stars of the burst are still inside their parent clouds. Indeed in these two objects t_0 is about equal to the time since burst ignition 0.05 Gyr. Conversely, for NGC 6090 the data show that the UV is not a negligible fraction of the total, implying for our model $t_G - t_{\text{burst}} > t_0 = 0.018$ Gyr. As a result stars with lifetime ≥ 18 Myr (corresponding to $M \lesssim 10 M_{\odot}$) are no more embedded within the clouds and contribute significantly to the ISRF. Actually the luminosity we ascribe to the diffuse cold component equals the warm one in NGC 6090, whereas it is 25% and 9% for M82 and Arp 220, respectively.

Calzetti, Kinney, & Storchi-Bergmann (1994) computed the "intrinsic depth" of the 2175 \AA dust absorption feature η (see their eq. [23]) in a number of starburst galaxies, finding that $-0.15 < \eta < 0$. For the three starbursts we find η ranging from -0.15 to -0.08 . Since the dust properties we adopt follow very well those of our Galaxy, at least in these objects the relative weakness of the 2175 \AA feature can be ascribed to the adopted geometry without invoking possible variations of extinction curve.

In conclusion for starbursts, the spectral coverage from UV to submillimeter wavelengths allows a robust evaluation of the luminosity of stars involved in the bursts and of the general interstellar radiation field. The latter is contributed by the long-lived stellar populations and by the stars produced in the burst but old enough to get out from the original MCs. Our model well describes the complexity of a starburst galaxy, and is flexible enough to reproduce the differences among them. It uses a reasonable number of parameters, which have a well-defined physical meaning and compare favorably to values derived from observations other than broadband spectra.

4.2. Spirals

The SEDs of three spiral galaxies, namely, M51, M100, and NGC 6946, have been well reproduced by our model. An interesting result is the significantly lower t_0 in spirals with respect to starbursting objects. This derives from their smaller observed ratios $L_{\text{FIR}}/L_{\text{UV}}$. In the three spirals analyzed here, the newly born SSPs quite soon get out from the parent clouds and significantly contribute to the heating of the diffuse dust. The expected contribution is larger for NGC 6946 and M100 than for M51. As a consequence, a

significant portion of the far-IR luminosity emitted by the diffuse dust (almost all for NGC 6946 and M100) should be inserted in the budget to infer the SFR in spiral galaxies, in agreement with the findings of Devereux et al. (1994) and Buat & Xu (1996). Taking this into account, the SFRs derived from the FIR luminosities through the conversion suggested by Kennicutt (1998) are in very good agreement with those used by the model.

The SFRs in our models, through the conversion of Kennicutt (1998) $L(\text{H}\alpha)(\text{ergs s}^{-1}) = 1.26 \times 10^{41} \times \text{SFR}(M_{\odot} \text{ yr}^{-1})$, yield H α luminosities of 7.6, 8.8, and $7.610^{41} \text{ ergs s}^{-1}$ for M51, M100, and NGC 6946, respectively, to be compared with observed values (Kennicutt, Tamblyn, & Congdon 1994, reported to our adopted distances) of 4.9, 5.0, and $2.2 \times 10^{41} \text{ ergs s}^{-1}$. These lower values would imply an internal H α extinction of $A_{\text{H}\alpha} = 0.5, 0.6,$ and 1.3 mag in the three spirals, consistent with the average value 1.1 adopted by Kennicutt (1998), based on a comparison of free-free radio and H α fluxes.

It is also worth noticing that masses in stars, dust, and gas derived by the model, as well as geometric parameters such as the disk scale length, are in good agreement with independent estimates. Our model includes the main physical aspects of star formation, stellar evolution, and dust absorption in spiral galaxies and allows a full use of the broadband data in order to explain their present status and their past history.

4.3. Ellipticals

The model with a relatively small number of parameters is able to produce a very good fit to the template SED of giant elliptical galaxies (see Fig. 13). Most excitement about spheroidal galaxies is related to their evolution. Indeed it has been suggested that, during the initial phases of star formation, they might look very similar to local violent starbursts (such as Arp 220), since the chemical enrichment and, as a consequence, the dust formation are very quick processes when SFRs are very high (Mazzei et al. 1994; Franceschini et al. 1994). This initial phase, if confined to

high enough redshifts $z \leq 2-2.5$, is the most natural way to produce the total energy and the shape of the far-IR background (Franceschini et al. 1991, 1994; Burigana et al. 1997), which has been tentatively detected by Puget et al. (1996) and recently confirmed by Hauser et al. (1998) and Fixsen et al. (1998). Also we expect that in the *ISO* extra deep surveys we may detect individual dusty spheroidal galaxies at substantial redshifts. Our model is able to describe in detail the evolution of elliptical galaxies in all the relevant range of frequencies and will be used for a comprehensive discussion of galaxy counts, related statistics, and astrophysical backgrounds.

4.4. Conclusion

We showed that the model and the related numerical code are extremely efficient in deriving a wealth of information from broadband spectra of starburst and spiral galaxies. Indeed, when SEDs from the UV to the submillimeter range are available, we are able to quantify the effects of dust reprocessing on observations, gaining information on very substantial quantities such as SFR, the IMF, and the past history of the galaxies. The model can be implemented in studies of local starburst and normal galaxies. It can also be used to trace back the history of the different classes of galaxies and, by confronting predictions and observations of number counts and redshift distributions in different bands, to understand their cosmological evolution. In particular we will use the model to investigate the role of dust during the early phase of galaxy formation, using available and forthcoming data on galaxy counts at wavelengths ranging from UV to radio bands.

Updated information on the code described in this study (GRASIL) can be found on the World Wide Web at <http://asterix.pd.astro.it/homepage/gian/>.

This work was supported by MURST and ASI under contract ARS-96-86. We are indebted to the anonymous referee for suggestions that led us to substantial improvements to the model and its presentation.

REFERENCES

- Acosta-Pulido, J. A., et al. 1996, *A&A*, 315, L121
Agladze, N. I., Sievers, A. J., Jones, S. A., Burlitch, J. M., & Beckwith, S. V. W. 1996, *ApJ*, 462, 1026
Anders, E., & Grevesse, N. 1989, *Geochim. Cosmochim. Acta*, 53, 197
Arimoto, N. 1996, in *ASP Conf. Ser. 98, From Stars to Galaxies: the Impact of Stellar Physics on Galaxy Evolution*, ed. C. Leitherer, U. Fritze-von-Alvensleben, & J. Huchra (San Francisco: ASP), 287
Bally, J., & Thronson, H. A., Jr. 1989, *AJ*, 97, 69
Beckman, J. E., Peletier, R. F., Knapen, J. H., Corradi, R. L. M., & Gentet, L. J. 1996, *ApJ*, 467, 175
Bertelli, G., Bressan, A., Chiosi, C., Fagotto, F., & Nasi, E. 1994, *A&AS*, 106, 275
Bianchi, S., Ferrara, A., & Giovanardi, C. 1996, *ApJ*, 465, 127
Binggeli, B., Sandage, A., & Tarenghi, M. 1984, *AJ*, 89, 64
Boulanger, F., & Viallefond, F. 1992, *A&A*, 266, 37
Bressan, A., Chiosi, C., & Fagotto, F. 1994, *ApJS*, 94, 63
Bressan, A., Granato, G. L., & Silva, L. 1998, *A&A*, 332, 135
Bruzual, A. G., & Charlot, S. 1993, *ApJ*, 405, 538
Bruzual, A. G., Magris, G., & Calvet, N. 1988, *ApJ*, 333, 673
Buat, V., Deharveng, J. M., & Donas, J. 1989, *A&A*, 223, 42
Buat, V., & Xu, C. 1996, *A&A*, 306, 61
Burigana, C., Danese, L., De Zotti, G., Franceschini, A., Mazzei, P., & Toffolatti, L. 1997, *MNRAS*, 287, L17
Calzetti, D. 1997, *AJ*, 113, 162
Calzetti, D., Kinney, A. L., & Storchi-Bergmann, T. 1994, *ApJ*, 429, 582
———, 1996, *ApJ*, 458, 132
Cardelli, J. A., Meyer, D. M., Jura, M., & Savage, B. D. 1996, *ApJ*, 467, 334
Carico, D. P., Sanders, D. B., Soifer, B. T., Elias, J. H., Matthews, K., & Neugebauer, G. 1988, *AJ*, 95, 356
Carico, D. P., Sanders, D. B., Soifer, B. T., Matthews, K., & Neugebauer, G. 1990, *AJ*, 100, 70
Cimatti, A., Bianchi, S., Ferrara, A., & Giovanardi, C. 1997, *MNRAS*, 290, L43
Code, A. D., & Welch, G. A. 1982, *ApJ*, 256, 1
Cohen, M., & Volk, K. 1989, *AJ*, 98, 1563
Considere, S., & Athanassoula, E. 1988, *A&AS*, 76, 365
de Jong, R. S., & van der Kruit, P. C. 1994, *A&AS*, 106, 451
Désert, F. X., Boulanger, F., & Puget, J. L. 1990, *A&A*, 237, 215
de Vaucouleurs, G., de Vaucouleurs, A., Corwin, J., Herold, G., Buta, R. J., Paturel, G., & Fouque, P. 1991, in *Third Reference Catalog of Bright Galaxies Vols. 1-3, XII*, (Berlin: Springer), 2069
Devereux, N. A., Price, R., Wells, L. A., & Duric, N. 1994, *AJ*, 108, 1667
Devereux, N. A., & Young, J. S. 1990, *ApJ*, 359, 42
———, 1992, *AJ*, 103, 1536
———, 1993, *AJ*, 106, 948
Doane, J. S., & Mathews, W. G. 1993, *ApJ*, 419, 573
Donas, J., Deharveng, J. M., Laget, M., Milliard, B., & Huguenin, D. 1987, *A&A*, 180, 12
Dorschner, J., & Henning, T. 1995, *A&A Rev.*, 6, 271
Draine, B. T., & Anderson, N. 1985, *ApJ*, 292, 494
Draine, B. T., & Lee, H. M. 1984, *ApJ*, 285, 89 (DL)
Draine, B. T., & Malhotra, S. 1993, *ApJ*, 414, 632
Dwek, E., et al. 1997, *ApJ*, 475, 565
Engargiola, G. 1991, *ApJS*, 76, 875
Evans, R. 1995, in *The Opacity of Spiral Disks*, ed. J. I. Davies & D. Burstein (Dordrecht: Kluwer), 281
Fioc, M., & Rocca-Volmerange, B. 1997, *A&A*, 326, 950
Fixsen, D. J., et al. 1998, in press
Franceschini, A., De Zotti, G., Toffolatti, L., Mazzei, P., & Danese, L. 1991, *A&AS*, 89, 285
Franceschini, A., Mazzei, P., De Zotti, G., & Danese, L. 1994, *ApJ*, 427, 140
Froehlich, H. E. 1982, *Astron. Nachr.*, 303, 97

- Genzel, R., et al. 1998, *ApJ*, 498, 579
 Gies, D. R., & Lambert, D. L. 1992, *ApJ*, 387, 673
 Gordon, M. A. 1990, *ApJ*, 350, L29
 Gordon, K. D., Calzetti, D., & Witt, A. N. 1997, *ApJ*, 487, 625
 Goudfrooij, P., de Jong, T., Hansen, L., & Norgaard-Nielsen, H. U. 1994, *MNRAS*, 271, 833
 Granato, G. L., & Danese, L. 1994, *MNRAS*, 268, 235
 Guhathakurta, P., & Draine, B. T. 1989, *ApJ*, 345, 230
 Guiderdoni, B., & Rocca-Volmerange, B. 1987, *A&A*, 186, 1
 Hauser, M. G., et al. 1998, in press
 Helou, G., Khan, I. R., Malek, L., & Boehmer, L. 1988, *ApJS*, 68, 151
 Hippelein, H., et al. 1996, *A&A*, 315, L79
 Ichikawa, T., van Driel, W., Aoki, T., Soyano, T., Tarusawa, K., & Yoshida, S. 1994, *ApJ*, 433, 645
 Ichikawa, T., Yanagisawa, K., Itoh, N., Tarusawa, K., van Driel, W., & Ueno, M. 1995, *AJ*, 109, 2038
 Im, M., Casertano, S., Griffiths, R. E., Ratnatunga, K. U., & Tyson, J. A. 1995, *ApJ*, 441, 494
 Impey, C. D., Wynn-Williams, C. G., & Becklin, E. E. 1986, *ApJ*, 309, 572
 Jura, M. 1986, *ApJ*, 306, 483
 Kennicutt, R. C., Jr. 1998, *ApJ*, 498, 541
 Kennicutt, R. C., Jr., Tamblyn, P., & Congdon, C. E. 1994, *ApJ*, 435, 22
 Kim, D.-W. 1989, *ApJ*, 346, 653
 Kim, S.-H., & Martin, P. G. 1996, *ApJ*, 462, 296
 Klaas, U., Haas, M., Heinrichsen, I., & Schulz, B. 1997, *A&A*, 325, L21
 Klein, U., Wielebinski, R., & Morsi, H. W. 1988, *A&A*, 190, 41
 Knapen, J. H., Cepa, J., Beckman, J. E., Soledad del Rio, M., & Pedlar, A. 1993, *ApJ*, 416, 563
 Knapp, G. R., Guhathakurta, P., Kim, D.-W., & Jura, M. A. 1989, *ApJS*, 70, 329
 Knapp, G. R., Helou, G., & Stark, A. A. 1987, *AJ*, 94, 54
 Krügel, E., & Siebenmorgen, R. 1994, *A&A*, 282, 407
 Lançon, A., & Rocca-Volmerange, B. 1996, *New Astron.*, 1, 215
 Laor, A., & Draine, B. T. 1993, *ApJ*, 402, 441
 Lees, J. F., Knapp, G. R., Rupen, M. P., & Phillips, T. G. 1991, *ApJ*, 379, 177
 Léger, A., d'Hendecourt, L., & Defourneau, D. 1989a, *A&A*, 216, 148
 Léger, A., Verstraete, L., d'Hendecourt, L., Dutuit, O., Schmidt, W., & Lauer, J. 1989b, in *IAU Symp. 135, Interstellar Dust*, ed. L. J. Allamandola & A. G. G. M. Tielens (Dordrecht: Kluwer), 173
 Leitherer, C., & Heckman, T. M. 1995, *ApJS*, 96, 9
 Lo, K. Y., Cheung, K. W., Masson, C. R., Phillips, T. G., Scott, S. L., & Woody, D. P. 1987, *ApJ*, 312, 574
 Malhotra, S., et al. 1996, *A&A*, 315, L161
 Mathis, J. S. 1990, *ARA&A*, 28, 37
 ———. 1996, *ApJ*, 472, 643
 Mathis, J. S., Mezger, P. G., & Panagia, N. 1983, *A&A*, 128, 212
 Mathis, J. S., & Whiffen, G. 1989, *ApJ*, 341, 808
 Matteucci, F. 1996, *Fundam. Cosmic Phys.*, 17, 283
 Mattila, K., Lemke, D., Haikala, L. K., Laureijs, R. J., Léger, A., Lehtinen, K., Leinert, C., & Mezger, P. G. 1996, *A&A*, 315, L353
 Mazzarella, J. M., & Boroson, T. A. 1993, *ApJS*, 85, 27
 Mazzei, P., De Zotti, G., & Xu, C. 1994, *ApJ*, 422, 81
 McLeod, K. K., Rieke, G. H., Rieke, M. J., & Kelly, D. M. 1993, *ApJ*, 412, 111
 Men'shchikov, A., & Henning, T. 1996, in *ESO Astrophysics Symposia, The Role of Dust in the Formation of Stars*, ed. H. U. Kaufl & R. Siebenmorgen (Berlin: Springer), 351
 Omont, A. 1986, *A&A*, 164, 159
 Puget, J. L., Abergel, A., Bernard, J. P., Boulanger, F., Burton, W. B., Désert, F. X., & Hartmann, D. 1996, *A&A*, 308, L5
 Puget, J. L., & Léger, A. 1989, *ARA&A*, 27, 161
 Puget, J. L., Léger, A., & Boulanger, F. 1985, *A&A*, 142, L19
 Rand, R. J., Kulkarni, S. R., & Rice, W. 1992, *ApJ*, 390, 66
 Rice, W., Lonsdale, C. J., Soifer, B. T., Neugebauer, G., Koplan, E. L., Lloyd, L. A., de Jong, T., & Habing, H. J. 1988, *ApJS*, 68, 91
 Rifatto, A., Longo, G., & Capaccioli, M. 1995, *A&AS*, 114, 527
 Rigopoulou, D., Lawrence, A., & Rowan-Robinson, M. 1996, *MNRAS*, 278, 1049
 Roberts, M. S., Hogg, D. E., Bregman, J. N., Forman, W. R., & Jones, C. 1991, *ApJS*, 75, 751
 Rowan-Robinson, M. 1979, *ApJ*, 234, 111
 ———. 1986, *MNRAS*, 219, 737
 ———. 1992, *MNRAS*, 258, 787
 Rybicky, G. B., & Lightman, A. P. 1979, *Radiative Processes in Astrophysics* (New York: Wiley)
 Sandage, A., & Tammann, G. A. 1975, *ApJ*, 196, 313
 Sanders, D. B., Soifer, B. T., Elias, J. H., Madore, B. F., Matthews, K., Neugebauer, G., & Scoville, N. Z. 1988, *ApJ*, 325, 74
 Sauvage, M., et al. 1996, *A&A*, 315, L89
 Scoville, N., & Young, J. S. 1983, *ApJ*, 265, 148
 Scoville, N. Z., Yun, M. S., & Bryant, P. M. 1997, *ApJ*, 484, 702
 Smith, J. 1982, *ApJ*, 261, 463
 Smith, C. H., Aitken, D. K., & Roche, P. F. 1989, *MNRAS*, 241, 425
 Snow, T. P., & Witt, A. N. 1995, *Science*, 270, 1455
 ———. 1996, *ApJ*, 468, L65
 Sofia, U. J., Cardelli, J. A., & Savage, B. D. 1994, *ApJ*, 430, 650
 Soifer, B. T., Sanders, D. B., Madore, B. F., Neugebauer, G., Danielson, G. E., Elias, J. H., Lonsdale, C. J., & Rice, W. L. 1987, *ApJ*, 320, 238
 Solinger, A., Morrison, P., & Markert, T. 1977, *ApJ*, 211, 707
 Solomon, P. M., Downes, D., Radford, S. J. E., & Barrett, J. W. 1997, *ApJ*, 478, 144
 Stark, A. A., Davidson, J. A., Platt, S., Harper, D. A., Pernic, R., Loewenstein, R., Engargiola, G., & Casey, S. 1989, *ApJ*, 337, 650
 Sturm, E., et al. 1996, *A&A*, 315, L133
 Tacconi, L. J., & Young, J. S. 1986, *ApJ*, 308, 600
 Tantaló, R., Chiosi, C., Bressan, A., & Fagotto, F. 1996, *A&A*, 311, 361
 Tsai, J. C., & Mathews, W. G. 1996, *ApJ*, 468, 571
 Tuffs, R. J., et al. 1996, *A&A*, 315, L149
 Tully, R. B. 1974, *J. AAVSO*, 27, 437
 van Driel, W., de Graauw, T., de Jong, T., & Wesselius, P. R. 1993, *A&AS*, 101, 207
 Veron-Cetty, M. P., & Veron, P. 1988, *A&A*, 204, 28
 Ward-Thompson, D., & Robson, E. I. 1990, *MNRAS*, 244, 458
 Wild, W., Harris, A. I., Eckart, A., Genzel, R., Graf, U. U., Jackson, J. M., Russell, A. P. G., & Stutzki, J. 1992, *A&A*, 265, 447
 Wise, M. W., & Silva, D. R. 1996, *ApJ*, 461, 155
 Witt, A. N., Thronson, H. A., & Capuano, J. M. 1992, *ApJ*, 393, 611
 Wynn-Williams, C. G., & Becklin, E. E. 1993, *ApJ*, 412, 535
 Xu, C., & De Zotti, G. 1989, *A&A*, 225, 12
 Young, J. S., Xie, S., Kenney, J. D. P., & Rice, W. L. 1989, *ApJS*, 70, 699